Membrane and Water Treatment, *Vol. 16, No. 1 (2025) 13-27*
https://doi.org/10.12989/mwt.2025.16.1.013

Empirical determination of Nusselt number for Flux prediction in DCMD process

Bora Shin[a], Jaewon Shin[b], Yanuar Chandra Wirasembada[c] and Jinwoo Cho[*]

Department of Environment and Energy, Sejong University, 209 Neungdong-ro, Gwangin-gu, Seoul 05006, Republic of Korea

(Received April 17, 2024, Revised October 9, 2024, Accepted October 10, 2024)

Abstract. This study aims to empirically derive a Nusselt number equation for predicting water flux in a direct contact membrane distillation (DCMD) system under varying cross flow velocities (CFV) and temperatures. The temperature of the bulk solution and the membrane surface differ due to the heat transfer coefficient. It is essential to determine the temperature of the membrane's surface using the heat transfer coefficient, which can be calculated using the Nusselt number, in order to predict the flux. The heat transfer coefficient varies due to various factors, which include membrane characteristics, operating conditions, module configurations, and overall system designs. The heat transfer coefficient varies depending on the characteristics of each system. Directly using previously reported Nusselt equations has limitations in predicting flux. It is necessary to derive an empirical equation for the system that was used in this study. One influential factor related to heat transfer is the CFV and temperature. Experiments were conducted under varying CFV (0.069–0.208 m/s) and temperatures (40–60°C), and an empirical Nusselt number equation was derived based on regression analysis of the experimental data, distinguishing between laminar and transition regions. A statistical analysis (t-test, MSE, MAPE) and accuracy evaluation through random experiments supported that the model accurately predicts the flux. The new Nusselt equation accurately predicted the flux with an error of only 3% (MAPE). This modeling approach can offer a method for empirically deriving a Nusselt equation suitable for each system and provides deeper insights into the relationships between flux, CFV, temperature, and heat transfer.

Keywords: cross flow velocity; heat transfer coefficient; membrane distillation; Nusselt number

1. Introduction

Membrane distillation (MD), which can treat saline water, saltwater, mine water, wastewater, reverse osmosis brine, and radioactive wastewater, is receiving a lot of attention as a potential technology for water treatment and purification (Abid *et al*. 2023). More than 6500 papers on membrane distillation were published in the last 15 years, which was from 2008 to 2002, and the number of publications has increased (Tai *et al*. 2023). This MD process is driven by the vapor pressure difference between the feed solution and the permeate solution using a hydrophobic membrane (Kim *et al*. 2017, Moreira *et al*. 2022, Moreira *et al*. 2023). The feed solution and the permeate solution flow across the hydrophobic membrane, and the liquid cannot pass through the membrane because of the hydrophobic membrane. Evaporation occurs on the membrane's surface of the high temperature feed side, and water vapor diffuses from the hot feed to the cold permeate through the porous membrane. Water vapor condenses on the cold permeate side to produce treated water (Andrjesdóttir *et al*. 2013, Gryta and Tomaszewska 1998, Loussif and Orfi 2016). The MD process has lower membrane fouling and offers a very high level of water treatment quality compared to reverse osmosis (RO), which experiences high membrane fouling due to high operating pressures (Lawson and Lloyd, 1997, Tibi *et al*. 2020). Furthermore, utilizing waste heat from the existing treatment processes to generate the driving force can make it a highly cost-effective process. MD can also utilize alternative energy sources, such as solar energy (Choi *et al*. 2022). The driving force of direct contact membrane distillation (DCMD) system is established by the temperature difference. Polarization of the temperature reduces the driving force for both mass transfer and heat transfer, which results in a decrease in water flux (Wang *et al*. 2023).

The performance of MD processes is influenced by various factors, which include membrane characteristics, operating conditions, module configurations, and overall system designs. Membrane characteristics include porosity, tortuosity, and thickness. High porosity reduces mass transport resistance, and it provides numerous pathways for vapor to traverse through the membrane, which results in high flux. The tortuosity and thickness characteristics are also important design factors in MD processes. A low tortuosity reduces the distance vapor molecules need to diffuse across the membrane, thus increasing flux. (Drioli *et al*. 2015). A shorter thickness is advantageous for vapor diffusion, but increased thermal conductivity leads to higher heat losses as the membrane thickness decreases, which results in reduced thermal efficiency of the membrane

[*]Corresponding author, Assistant Professor,
E-mail: jinwoocho@sejong.edu
[a] Ph.D., E-mail: glgl1770@naver.com
[b] Ph.D., E-mail: hyehj0@hanmail.net
[c] Ph.D., E-mail: yanuarchandraw@gmail.com

ISSN: 2005-8624 (Print), 2092-7037 (Online)

(González *et al*. 2017). The thermal conductivity of membranes is also a factor that influences flux. If the thermal conductivity of the membrane is high, it can lead to a decrease in flux due to the temperature polarization, which results in reduced energy efficiency of the MD process (Al-Obaidani *et al*. 2008). The heat lost (Q_f) from the bulk of the feed water to the membrane surface on the feed side is equal to the sum of the latent heat of vaporization within the membrane (Q_v , heat of vaporization) and the heat across the membrane material and its gas-filled pores (Q_c, conduction). As a result, there is a difference in temperature between the bulk solution of the feed and the membrane surface on the feed side.

One of the influencing factors among the factors related to heat transfer and operating conditions is cross flow velocity (CFV). A higher CFV leads to an increased heat transfer coefficient (h_f) at the feed side, which results in higher heat transfer rates from the bulk of the feed to the membrane surface (Khayet *et al*. 2011). It is therefore possible to reduce temperature polarization near the membrane surface and expect a higher flux by employing a higher CFV (Alkhudhiri *et al*. 2012, Phattaranawik *et al*. 2003b).

It is necessary to calculate the temperatures on both sides of the membrane surface ($T_{m,f}$ and $T_{m,p}$) using the heat transfer coefficients on the feed side and permeate side (h_f and h_p) in order to predict flux. Heat transfer coefficient can be calculated using the Nusselt number (Nu) to establish the correlation between Nu and the heat transfer coefficient (Bergman *et al*. 2011, Gryta and Tomaszewska 1998). The Nusselt number is a dimensionless constant that is defined as the ratio of convective heat transfer to conductive heat transfer across the boundary layer of the membrane surface (Yunus 2019). The Nusselt number (Nu) can be expressed as a function of Reynolds number and Prandtl number. The Nusselt number therefore varies based on the factors, such as Reynolds number (Re), which includes CFV, and the module's characteristic hydraulic diameter (d_h), which results in different heat transfer coefficients. It is necessary for these reasons, to empirically determine the appropriate Nusselt number for each specific module and system (Kim *et al*. 2018). Research has been reported over the years to derive empirical expressions for the optimal Nusselt number thar is suitable for each system (Andrjesdóttir *et al*. 2013, Chauhan and Tyagi 2023, Gryta *et al*. 1997, Izquierdo-Gil *et al*. 2008, Kim *et al*. 2018, Schofield *et al*. 1987).

In this study, a useful method is presented for enhancing the accuracy of flux predictions by empirically deriving a Nusselt equation suitable for each system, considering the effects of CFV and temperature by distinguishing between laminar and transitional flow regions. The empirical Nusselt equations reported in previous studies were utilized to predict the flux for each experimental condition in this study. However, discrepancies were observed between the predicted values and the observed values. To predict flux, empirical Nusselt equations suitable for DCMD have been studied (Alkhudhiri *et al*. 2012, Kim *et al*. 2018, Martínez-Díez and Vazquez-Gonzalez 1999, Phattaranawik *et al*. 2003b, Sieder and Tate 1936, Srisurichan *et al*. 2006). But, these equations are not absolute and can vary significantly depending on the flow system and module geometry (Hitsov *et al*. 2015). Additionally, previous studies reported Nusselt equations limited to laminar flow regions or turbulent flow regions. The transitional flow region was either excluded or empirically derived within the laminar flow range (Alkhudhiri *et al*. 2012, Kim *et al*. 2018, Martínez-Díez and Vazquez-Gonzalez 1999, Phattaranawik *et al*. 2003b, Sieder and Tate 1936, Srisurichan *et al*. 2006). Therefore, it is necessary to derive an empirical equation suitable for the system under study by distinguishing between laminar and transitional flow. The experiments were conducted in this study in order to observe the changes in the heat transfer coefficient and flux with variations in the CFV (0.069-0.208 m/s) and feed temperature (40-60°C). The observed heat transfer at various CFV values exhibited different slopes in the laminar layer and transition region. Therefore, a new Nusselt number equation suitable for this system was derived by distinguishing between laminar flow and the transition region. The accuracy of the flux prediction was evaluated by conducting distillation experiments under different feed temperature conditions (55°C). This modeling approach can offer a method for empirically deriving a Nusselt equation suitable for each system by distinguishing between laminar and transitional flow regions. Also, it provides deeper insights into the relationships between flux, CFV, temperature, and heat transfer.

2. Theoretical model development

2.1 Mass and heat transfer equations

In the DCMD module, the feed and permeate solutions flow in opposite directions across the membrane, as depicted in Fig. 1. In an operating DCMD system, heat transfer and mass transfer occur simultaneously. The vaporized water from the feed passes through the membrane and moves to the permeate, generating flux (J_w, mass transport). The water flux (J_w) of a DCMD system can be calculated using the following equation (Andrjesdóttir *et al*. 2013, Khayet *et al*. 2011, Termpiyakul *et al*. 2005)

$$J_w = B_w\left(P^0_{w,f} - P^0_{w,P}\right) \tag{1}$$

$P^0_{w,f}$ and $P^0_{w,P}$ represent the pure vapor pressures of water in the feed and permeate, respectively. The pure vapor pressure of water at different temperatures can be determined using the Antoine equation (Chauhan and Tyagi 2023, Khayet *et al*. 2011)

$$p^0_w(\mathrm{T}) = \exp\left(23.1964 - \frac{3816.44}{T - 46.13}\right) \tag{2}$$

B_w represents the membrane permeability ($kg \cdot m^{-2} \cdot s^{-1} \cdot Pa^{-1}$), and the diffusion of water within the membrane occurs via the mechanism of the combined knudsen/ molecular diffusion, which makes it possible to calculate the water's permeability (B_w) using the following equation (Curcio and Drioli 2005, Khayet *et al*. 2011).

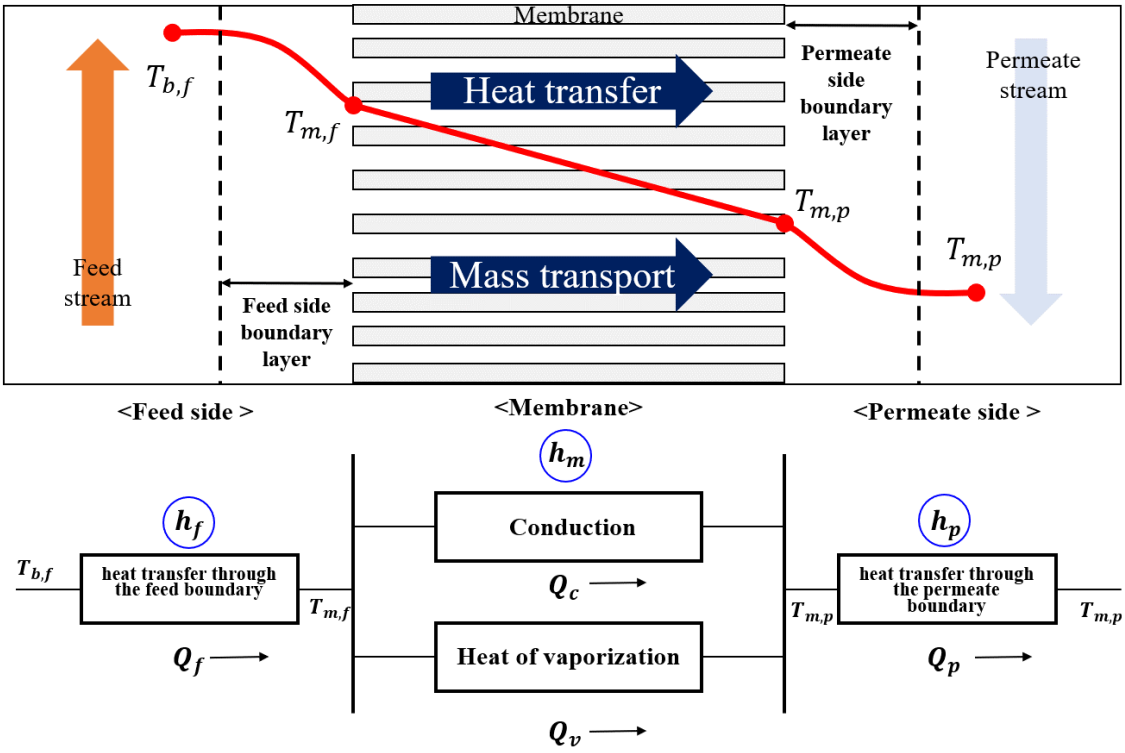

Fig. 1 Schematic representation of Heat transfer in DCMD

$$B^c = \frac{1}{RT\delta}\left[\frac{3}{2}\left(\frac{\pi M_w}{8RT}\right)^{\frac{1}{2}} + \frac{P_a\tau}{\varepsilon P D_w}\right]^{-1} \quad (3)$$

M_w represents the molecular weight of the water, P_a is the pressure in the membrane pore, δ is the thickness of the membrane, and τ is the tortuosity. D_w represents the diffusion coefficient of H_2O molecules in the air, and PD_w can be calculated using Eq. (4) (Khayet *et al*. 2011, Khayet *et al*. 2004, Phattaranawik *et al*. 2003a)

$$PD_w = 1.895 \times 10^{-5}\, T^{2.072} \quad (4)$$

Heat transfer occurs due to the latent heat (Q_v) generated during the vaporization and mass transfer through the membrane, as well as the conductive heat transfer (Q_c) related to the membrane thickness and thermal conductivity. As a result, a boundary layer is formed between the bulk fluid and the membrane on both sides, causing a temperature loss (Fig. 1). Fig. 1 illustrates that heat transfer is described in three steps, which include (i) heat transfer through the feed boundary layer (Q_f), (ii) heat transfer through the membrane (Q_m), and (iii) heat transfer through the permeate boundary layer (Q_P). The heat transfer in each step is in balance with the energy at steady-state conditions, which is depicted below (Khayet *et al*. 2011). It is assumed that the system reaches a steady state under the initially set operating conditions. Additionally, the fluid flow is considered incompressible, and heat loss through the acrylic module body is neglected.

$$Q_f = Q_m = Q_p \quad (5)$$

The heat transfer through the membrane (Q_m) is by conduction (Q_c) and latent heat (Q_v). The heat transfer for the feed side, membrane, and permeate side can be expressed using the equation below by applying the heat transfer coefficient (h) to each side:

$$\begin{aligned} h_f(T_{b,f} - T_{m,f}) &= \frac{k_m}{\delta}(T_{m,f} - T_{m,p}) + J_w \Delta H_{v,w} \\ &= h_p(T_{b,p} - T_{m,p}) = \mathrm{H}(T_{b,f} - T_{b,p}) \end{aligned} \quad (6)$$

where h_f and h_p are the heat transfer coefficients in the feed and permeate boundary layers, respectively, and k_m is the thermal conductivity of the membrane. H is the global heat transfer coefficient of the DCMD process (Khayet *et al*. 2011). The heat transfer through the boundary layers is recognized as the limiting factor of the DCMD efficiency. The temperature of the membrane boundary ($T_{m,f}$ and $T_{m,p}$) differs from the temperature of the bulk solution ($T_{b,f}$ and $T_{b,p}$) (Lawal and Khalifa 2014), which is due to the presence of boundary layers adjoining the membrane surfaces at both the feed and permeate sides. The temperature polarization coefficient (TPC) is defined as (Drioli *et al*. 2015, Phattaranawik *et al*. 2003b):

$$\mathrm{TPC}(\theta) = \frac{T_{m,f} - T_{m,p}}{T_{b,f} - T_{b,p}} \quad (7)$$

A TPC value close to 1.0 indicates that the temperature difference between the membrane surface on the feed side and the permeate side is approximately equal to the temperature difference between the bulk solution on the feed side and the permeate side. In other words a higher

Table 1 Nusselt number equation derived from the previous research.

No.	Flow regime	Empirical equations	Eq.
(a)	Laminar (Re < 2100)	$1.86\left(Re\,\mathrm{Pr}\frac{d_h}{L}\right)^{0.33}$	(16)
(b)	Laminar	$1.86Re^{0.96}Pr^{1/3}\left(\frac{d_h}{L}\right)^{1/3}$	(17)
(c)	Laminar 150 < Re < 3500	$0.298Re^{0.646}Pr^{0.316}$	(18)
(d)	Laminar (Re < 2100)	$3.66+\frac{0.104\,Re\mathrm{Pr}\,(\frac{d_h}{L})}{1+0.0106\left(RePr(d_h/L)\right)^{0.8}}$	(19)
(e)	-	$0.0871e^{-0.027\,T}RePr^{c}$ (c is 0.3 for feed side, 0.4 for permeate side)	(20)
(f)	Turbulent flow ($2500<Re<1.25\times 10^5$) $0.6<Pr<100$	$\mathrm{Nu}=0.023Re^{0.8}Pr^{n}$ (n=0.4 for heating, n=0.3 for cooling)	(21)

*(a) Eq. (16) (Alkhudhiri *et al*. 2012, Andrjesdóttir *et al*. 2013, Martínez-Díez and Vazquez-Gonzalez, 1999, Sieder and Tate, 1936, Srisurichan *et al*. 2006), (b) Eq. (17) (Alkhudhiri *et al*. 2012, Izquierdo-Gil *et al*. 2008), (c) Eq. (18) (Gryta *et al*. 1997), (d) Eq. (19) (Andrjesdóttir *et al*. 2013, Phattaranawik *et al*. 2003a, Thomas, 1992), (e) Eq. (20) (Kim *et al*. 2018), and (f) Eq. (21) (Srisurichan *et al*. 2006)

TPC value indicates a decreased formation of temperature polarization through the boundary layer between the bulk solution and the membrane surface (Kim *et al*. 2018).

The temperature at the surface of the membrane in the feed side and the temperature at the surface of the membrane in the permeate side can be determined from using the equation below.

$$T_{m,f} = \frac{\frac{k_m}{\delta}\left(T_{b,f}+\frac{h_f}{h_p}T_{b,f}\right)+h_fT_{b,f}-J_w\Delta H_w}{\frac{k_m}{\delta}+h_f\left(1+\frac{k_m}{\delta h_p}\right)} \quad (8)$$

$$T_{m,p} = \frac{\frac{k_m}{\delta}\left(T_{b,f}+\frac{h_p}{h_f}T_{b,p}\right)+h_pT_{b,p}-J_w\Delta H_w}{\frac{k_m}{\delta}+h_p\left(1+\frac{k_m}{\delta h_f}\right)} \quad (9)$$

To predict the flux in DCMD while accounting for heat transfer using the above equation, it is necessary to derive the heat transfer coefficient (h) by applying the appropriate Nusselt equation for the DCMD system. The Nusselt number (Nu) is a dimensionless quantity used in heat transfer to characterize the ratio of convective to conductive heat transfer across a fluid boundary layer (Incropera *et al*. 1996). The Nusselt number can be expressed as a function of the Reynolds number and the Prandtl number, as shown in Eq. (10) (Khayet and Matsuura, 2011, Kim *et al*. 2018). The heat transfer coefficient on the feed and permeate sides can be calculated using the Nusselt number (Nu) and the Prandtl number (Pr) based on the Reynolds number (Re). Where k is the thermal conductivity of fluid, d_h is the hydraulic diameter and h is the heat transfer coefficient (Lawson and Lloyd 1997). μ is viscosity, C_p is the specific heat capacity, and d is density. u is velocity (= Cross flow velocity, CFV). L is channel length (Phattaranawik *et al*. 2003b)

$$\mathrm{Nu}=\mathrm{f}(\mathrm{Re},\mathrm{Pr})=aRe^{b}Pr^{c} \quad (10)$$

$$Nu_f=\frac{h_fd_h}{k_f} \quad (11)$$

$$Nu_p=\frac{h_pd_h}{k_p} \quad (12)$$

$$\mathrm{Pr}=\frac{\mu C_p}{k} \quad (13)$$

$$\mathrm{Re}=\frac{\rho ud}{\mu} \quad (14)$$

$$d_h=\frac{4Ac}{Pe} \quad (15)$$

The heat transfer coefficient is affected by several parameters, which include the cross-sectional area of the module flow (A_c), the length of the wall that is in contact with water (Pe), the cross-flow velocity (CFV), the density (ρ), the hydraulic diameter (d_h), the viscosity (μ), the specific heat (C_p), and the thermal conductivity of the membrane (k_m) (Khayet *et al*. 2011, Lawson and Lloyd 1997). Some studies were conducted to derive empirical equations, which is shown Table 1 (Alkhudhiri *et al*. 2012, Kim *et al*. 2018, Martínez-Díez and Vazquez-Gonzalez

Table 2 Properties of the membrane (GVHP, Millipore)

Parameter	Unit	Value
Thermal conductivity of the membrane (Km)	W/m·K	0.041
Thickness of membrane (δ)	m	0.000125
Pore size ($\boldsymbol{d_p}$)	um	0.22
Tortuosity (τ)	-	2.083
Porosity (ε)	-	0.75
Effective area of the membrane ($\boldsymbol{A_m}$)	m^2	0.0021

1999, Phattaranawik *et al*. 2003b, Sieder and Tate 1936, Srisurichan *et al*. 2006). The Nusselt number is a semi-empirical correlation used to estimate the heat transfer coefficient in water (Hitsov *et al*. 2015). However, this form is not absolute and can vary significantly depending on the flow system and module geometry (Hitsov *et al*. 2015). The parameters influencing heat transfer in the DCMD system and their relationships are not yet fully understood (Yazgan-Birgi *et al*. 2019). Key factors such as the application of the Nusselt equation in the fluid's transitional region, changes in heat transfer rate due to inlet flow, unaccounted heat losses, and variations in the Nusselt number based on module size are still under investigation (Dudchenko *et al*. 2020). A comprehensive Nusselt equation that addresses all these factors is yet to be developed. Among these factors, the temperature of the solution affects parameters such as the vapor pressure of the feed permeate (the driving force of DCMD), density (ρ), viscosity (μ), and specific heat (C_p), ultimately impacting the flux. Additionally, the operating condition of CFV affects the Reynolds number, so changes in the CFV of the feed and permeate in the DCMD system also influence the heat transfer coefficient (Eqs. (10)-(12)). Furthermore, when transitioning from laminar flow to the transitional region, the formation of eddy currents activates more intense mixing and enhances the energy of the fluid, resulting in an increased heat transfer rate (Incropera *et al*. 1996). Therefore, the changes in heat transfer rates between laminar and transitional flow will be experimentally examined, and the results will be discussed in Section 4.

2.2 Flux calculation procedure

It is necessary to determine the temperature of each surface of the membrane ($T_{m,f}$ and $T_{m,p}$) to calculate the flux. The bulk temperatures of the feed and permeate streams ($T_{b,f}$ and $T_{b,p}$) differ from the temperatures near the membrane's surfaces in the DCMD system, which is due to heat transfer resistances. Furthermore, the surface temperatures on both sides of the membrane can be calculated by substituting the flux values that are shown in Eqs. (8)-(9), which represent the latent heat flow from the feed to the permeate side. The procedure, which is depicted in Fig. 2, was utilized to compute the water flux.

In the initial stage, the bulk temperatures of the feed and permeate were assumed as $T_{m,f}$ and $T_{m,p}$ respectively. The vapor pressure (P_f^0 and P_p^0) and the permeability coefficient (B) at the given temperature were calculated using Eqs. (2)-(3). The flux is calculated using Eq. (1). The calculated flux value was used to compute $T_{m,f}^*$ and $T_{m,p}^*$ using Eqs. (8)-(9). $T_{m,f}^*$ and $T_{m,p}^*$ were subsequently compared with the initially set values of $T_{m,f}$ and $T_{m,p}$. If the error between these two values exceeded 0.1%, the process was reset to the initial stage, with the $T_{m,f}^*$ and $T_{m,p}^*$ values from the previous step being assigned as the new $T_{m,f}$ and $T_{m,p}$. values. This iterative process was repeated using the procedure that is depicted in Fig. 2. The iterations continued until the absolute difference between $T_{m,f}^*$, $T_{m,}^*$ and $T_{m,f}$, $T_{m,p}$ was less than 0.001. Finally, the obtained $T_{m,f}$ and $T_{m,p}$values were used to calculate the flux.

3. Materials and methods

3.1 Direct contact membrane distillation system

A schematic diagram of this device is shown in Fig. 3. A DCMD system was constructed on a scale of 2 L/day. The feed water was heated in a water bath, while the permeate water was maintained at a temperature of 20 °C using a chiller. A PVDF membrane (GVHP, Millipore) from Millipore Corp was utilized for the experiment. Table 2 presents the thermal conductivity of the membrane, the pore size, porosity, and thickness of the membrane (Kim *et al*. 2018, Phattaranawik *et al*. 2003b). A schematic diagram of the module configuration is shown in Fig. 3(b). The membrane is positioned at the center of the module, which includes a hot feed solution stream flowing in one direction and a cold permeate solution stream flowing in the opposite direction. The feed solution (40, 50, 60 °C) was heated with a Scilab SB-11 water bath from Korea, and it was continuously introduced into the module using a ColeParmer console drive gear pump from the USA. The flow meter was installed from Dwyer to measure the flow rates of the feed and permeate entering the system.The permeate solution was simultaneously cooled using a circulation system (Scilab SCR-P12, Korea) flowing counter to the feed solution within the module. The temperatures in both the feed and permeate were measured using multimeters (WTW, TetraCon® 925, Germany). The temperature was measured in the bulk solution, with the assumption that heat loss up to the module inlet is neglected. The mass of the condensed liquid on the permeate water side was measured every 3 minutes using a balance (Ohaus, arg4202, Germany). The flux value was calculated by substituting the measured mass of the permeate water into Eq. (22)

$$\mathrm{J} = \frac{Q_w}{A_m} = \frac{\Delta m}{\rho_w A \Delta t} \tag{22}$$

3.2 Experimental Estimation of Nu Number

Distillation experiments were conducted using deionized water at different CFV and temperatures to determine the suitable Nusselt number. The feed side temperatures were set at 40, 50, and 60 °C, and the CFV was set at 0.069, 0.104,

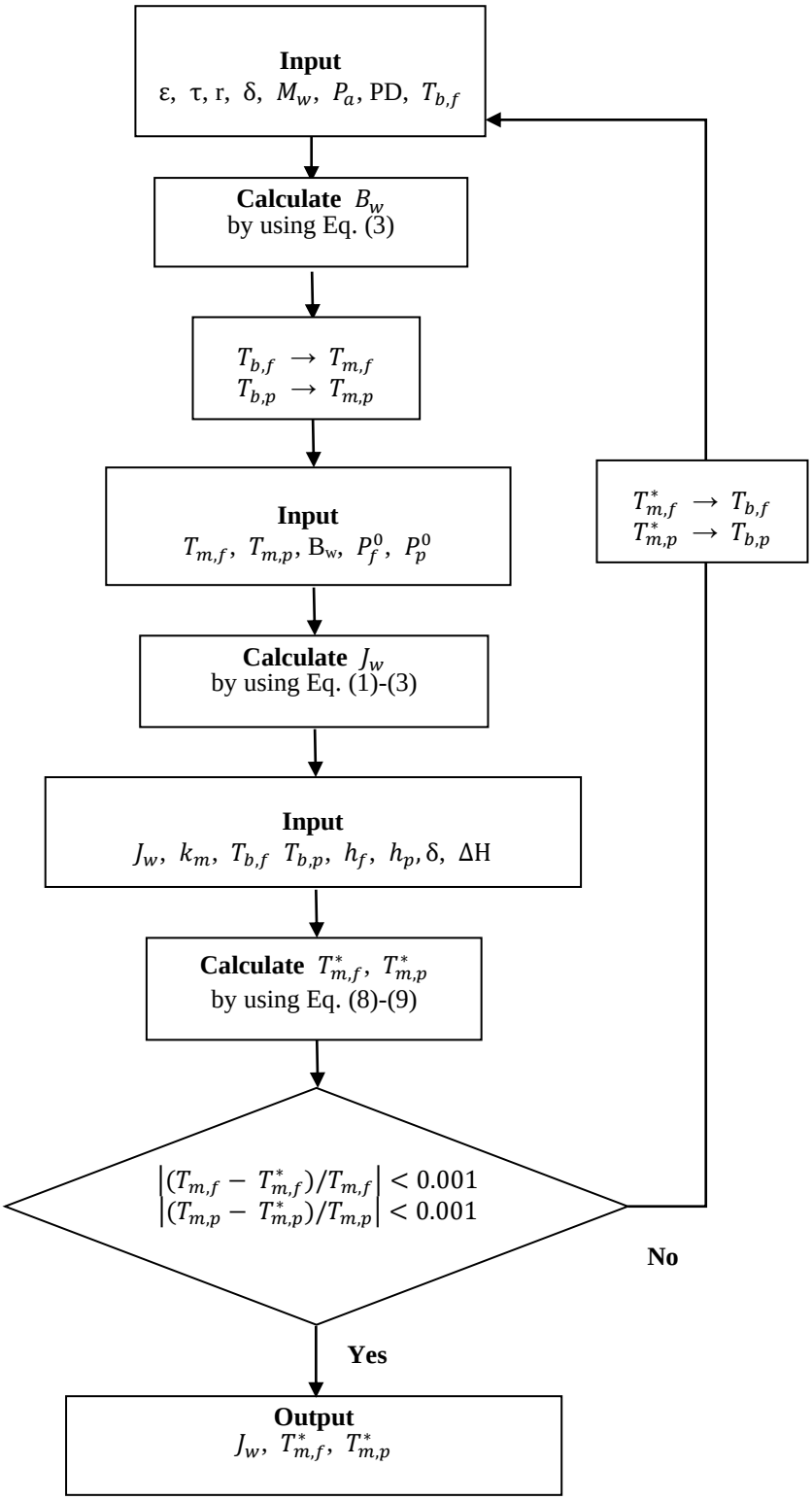

Fig. 2 Scheme of the iteration procedure on the flux computation

0.125, 0.156, 0.181, 0.194, 0.201, and 0.208 m/s for each temperature condition. A total of 24 sets of flux data were observed. The distillation test was conducted twice under the same conditions, and the average value was used. Based on a Reynolds number of 2300, the flow was categorized into laminar and transition regimes depending on the temperature and CFV conditions of each experiment. A new Nusselt number equation was derived for each case using regression analysis with the average experimental data, utilizing the SigmaPlot program.

To validate the developed model, additional experiments were conducted under the following random temperature

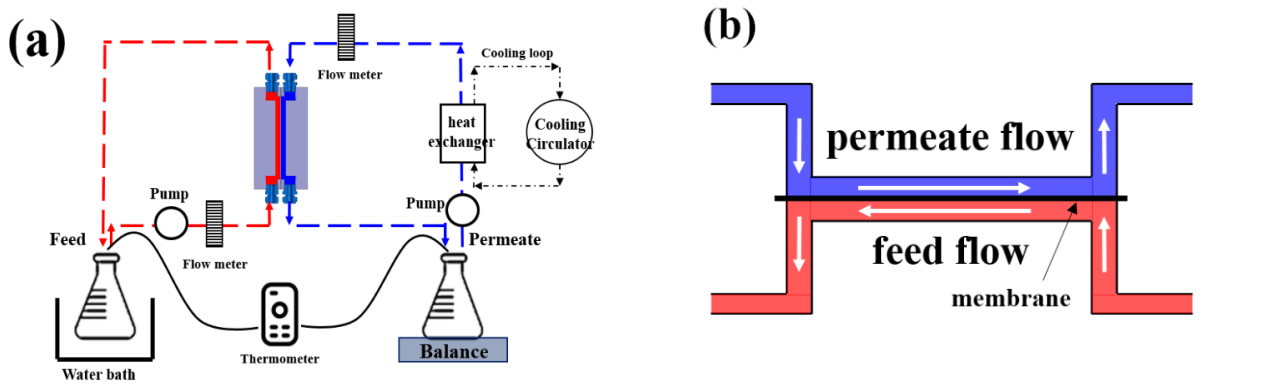

(a) Schematic of a DCMD system (b) Schematic side view of the membrane module

Fig. 3 Schematic of DCMD system and membrane module

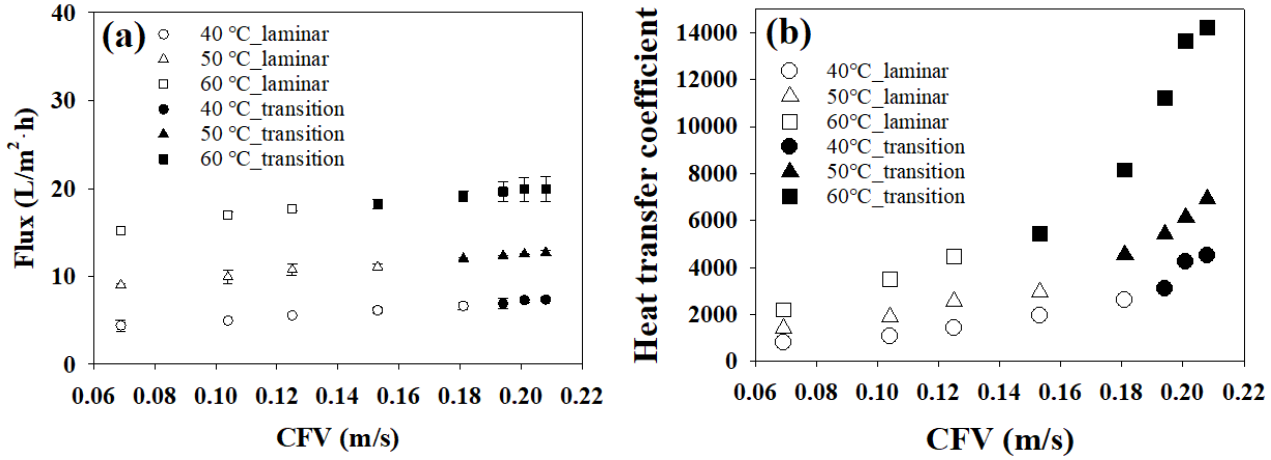

(a) Observed flux (L/m^2·h) (b) heat transfer coefficient of feed (W/m^2·K)

Fig. 4 Experimental results for temperatures of 40, 50, and 60 ℃ under various CFV conditions

conditions: a temperature of 55°C and eight different cross flow velocities ranging from 0.069 to 0.208 m/s. The observed fluxes from this experiment were compared with the fluxes predicted by the model using new Nusselt equations through a statistical analysis (t-test). A t-test was performed with a 95% confidence interval to validate the reliability of the model. Additionally, the accuracy of the model was verified using MSE and MAPE.

3.3 Model validation method

To validate the accuracy of the developed model, the mean squared error (MSE) and mean absolute percentage error (MAPE) were analyzed. (Shin *et al*. 2024). The MSE, which stands for mean squared error, is a metric used to evaluate the performance of a prediction model:

$$MSE = \frac{\sum(predicted\ value - observed\ value)^2}{number\ of\ data\ point\ (n)} \quad (23)$$

MAPE is a metric used to measure the accuracy of a forecasting model. It represents the average of the absolute percentage differences between the predicted values and the actual observed values. The formula for MAPE is:

$$MAPE = \frac{1}{n}\sum\left|\frac{(predicted\ value - observed\ value)}{observed\ value}\right| \times 100\% \quad (24)$$

3.4 Sensitivity analysis

The sensitivity analysis was conducted to assess the stability of the developed model and to simulate the impact of the targeted parameters on flux in this study. The factors selected for sensitivity analysis were the operating conditions of temperature and CFV, as well as the membrane property Km. All other factors were fixed at initial values while the values of target factors were varied from − 50% to + 50% of the initial value. The sensitivity of the targeted parameter was defined as follows:

$$S(i) = \frac{J(i) - J_0}{J_0} \times 100\% \quad (25)$$

i refers to the target parameter, S(i) indicates the sensitivity of parameter i to the predicted flux, J(i) represents

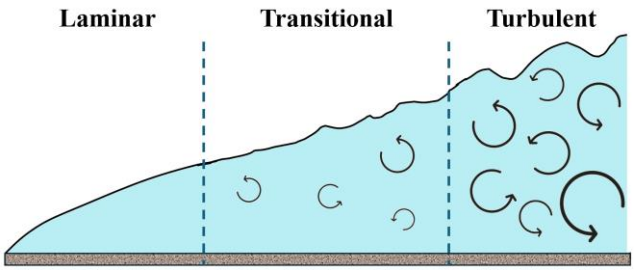

Fig. 5 Fluid mixing in each flow regime

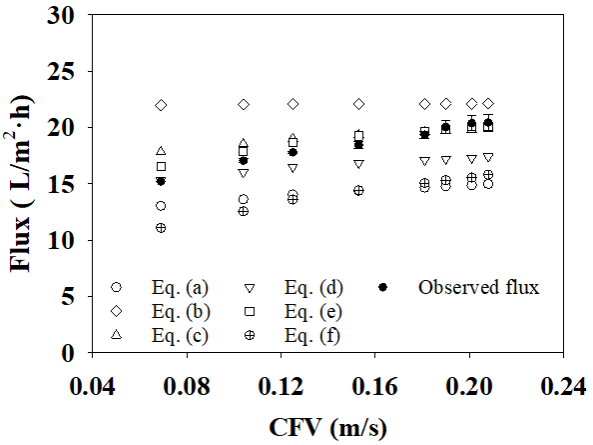

Fig. 6 Comparison between the observed flux in this study and the predicted flux of the previous empirical Nu formula, which is listed in Table 1

the predicted flux when the value of parameter i is varied from −50% to +50% of its original value, with all other parameters held constant, and J_0 is the initial values for all parameters (Conditions: 0.125 m/s, feed temperature of 60 °C, Km of 0.041 W/m·K).

4. Results and discussions

4.1 Effect of cross flow velocity

Distillation experiments were conducted under three temperature conditions (40, 50, 60°C) and eight different CFV conditions (0.069, 0.104, 0.125, 0.153, 0.181, 0.194, 0.201, 0.208). At a feed temperature of 40°C, the water flux increased from 4.41 to 7.36 LMH as the CFV increased. At a feed temperature of 50°C, the water flux increased from 9 to 12.7 LMH as the CFV increased. Under the 60°C condition, the flux increased from 15.18 to 19.96 LMH as CFV increased. The experimental results are presented in Fig. 4(a). The flux of the water also increased as the temperature and CFV increased. The increase in flux as the temperature rises is due to Antoine's law, which leads to a rise in the vapor pressure of the feed solution as its temperature increases (Alkhudhiri *et al*. 2012, Andrjesdóttir *et al*. 2013, Lawson and Lloyd 1997). In other words, as the temperature of the feed increases, the vapor pressure of the feed, which serves as the driving force in MD, also increases. As a result, an increase in flux was observed with rising temperatures. The reason flux increases with higher CFV is that, at the same feed temperature, the heat transfer coefficient increases as CFV rises. As the cross-flow velocity (CFV) increases, the Reynolds number (Re) also rises. A higher Reynolds number enhances the heat transfer rate, reducing thermal polarization and increasing the vapor pressure gradient across the membrane (Phattaranawik *et al*. 2003b). This results in a greater ΔP_m, allowing more vapor to permeate the membrane (mass transport), thereby increasing flux. The relationship between CFV, heat transfer, and flux will be explained in detail in the following paragraph.

The bulk temperature of the feed side ($T_{b,f}$) and the temperature of the membrane surface ($T_{m,f}$) differ due to heat transfer resistance, which leads to the occurrence of temperature polarization (Curcio and Drioli 2005). Heat transfer occurs according to the following equation in a steady-state condition (Gryta and Tomaszewska 1998, Khayet *et al*. 2011).

$$dQ_f = h_f(T_{b,f} - T_{m,f})\mathrm{dA} = \mathrm{dQ}_C + dQ_V = h_p(T_{b,p} - T_{m,p}) = q_m dA = dQ \quad (26)$$

The heat transfer coefficients (h_f and h_p) for both the feed and the permeate were calculated by combining the observed flux with Eqs. (8)-(12). q_m represents the heat flux through the membrane. A is the membrane's surface area. As seen in Eqs. (26), changes in the heat transfer coefficient affect the heat transfer ($Q_c + Q_V$) through the membrane. At this point, Q_v is related to the mass transport (J_w) and the latent heat associated with the vaporized molecules. As the cross flow velocity increases, the fluid contacts the membrane surface at a faster flow rate, resulting in heat being transferred more quickly across the boundary layer at the membrane surface. As a result, a substantial temperature gradient is maintained on both sides, sustaining a high flux (Khayet and Matsuura, 2011, Lawson and Lloyd, 1997). That is, as the CFV increases, the thermal boundary layer (the layer with a temperature gradient formed between the bulk of the feed and the membrane surface) becomes thinner, resulting in enhanced heat transfer efficiency. (Hitsov *et al*. 2015, Yazgan-Birgi *et al*. 2019). Therefore, as the fluid velocity increases, the heat transfer coefficient also increases (Gryta *et al*. 1997), which can also be observed in Eqs. (10)-(11), and (14). As a result, the temperature gradient across the membrane increases, leading to a rise in the vapor pressure difference (ΔP_m), thereby increasing the flux. However, the increase in the heat transfer coefficient with CFV does not lead to an infinite increase in the flux of DCMD. As the CFV increases, heat transfer occurs more efficiently, resulting in an increase in flux within the vapor pressure range that can be generated at the bulk temperature. An increase in CFV enhances the vapor pressure gradient across the membrane, but the absolute magnitude of heat transfer is governed by the bulk temperature (Dudchenko *et al*. 2020, Leitch *et al*. 2017, Phattaranawik *et al*. 2003b).

The heat transfer coefficients experimentally determined under eight different CFV conditions across the laminar to transitional flow range for each temperature are shown in Fig. 4(b). As the CFV increased, the heat transfer coefficient (h) also increased, however, based on the Reynolds number,

Table 3 Evaluation of the accuracy of the observed and predicted using the existing Nu equation (a)-(f)

Nusselt number Eq.	MSE	MAPE (%)
(a)	17.2	21.7
(b)	16.4	21.4
(c)	1.6	5.5
(d)	3.4	8.6
(e)	1.1	4.6
(f)	17.4	22.9

the rate of increase of the heat transfer coefficient became steeper as the transitional flow regime was approached. This is because more intense mixing of the fluid occurs as it transitions from the laminar flow to the transitional region Also heat transfer increases as the fluid's energy becomes more active, as shown in Fig. 5. (Incropera *et al*. 1996). Promoting the generation of eddy currents enhances fluid flow instability and improves heat transfer (Khayet and Matsuura 2011, Lawson and Lloyd 1997). Therefore, this experiment highlighted the necessity of using appropriate Nusselt equations for predicting flux in both the laminar and transitional flow regimes.

4.2 Flux prediction using the previous empirical Nu formula

During MD operation, heat transfer occurs simultaneously with mass transfer, which generates flux. To accurately predict the flux, it is essential to understand the heat transfer within the system. It is difficult to directly measure the temperature on the membrane's surface of a DCMD system. Therefore, the heat transfer coefficient must be calculated using the empirical Nusselt equation, which is then used to predict the temperatures on both sides of the membrane in order to calculate the flux (Khayet *et al*. 2011). To estimate the heat transfer coefficient under a fixed set of operating conditions in a specific MD module, various empirical Nusselt number (Nu) equations have been reported. (Alkhudhiri *et al*. 2012, Andrjesdóttir *et al*. 2013, Gryta *et al*. 1997, Kim *et al*. 2018, Phattaranawik *et al*. 2003a, Srisurichan *et al*. 2006).

Fig. 6 compares the observed flux under the 60 °C experimental condition in this study with the flux predicted using the previously reported Nu equations. The results of the accuracy evaluation, which assessed whether the predicted flux using the existing Nusselt equation accurately predicts the observed values from this experiment, are shown in Table 3. The accuracy analysis results show that the MAPE values for Eqs. (a), (b), and (d) were 21.7%, 21.4%, and 8.6%, respectively, indicating a significant error compared to the observed values. Eq. (c), which was empirically derived to include the laminar region and the transitional region up to a Reynolds number of 3500, showed a MAPE of 5.5%. However, as CFV decreased, the accuracy of flux prediction declined. Eq. (e) was derived by fitting the experimental results across both the laminar and transitional flow regimes, leading to larger errors in flux prediction as CFV decreased. In the graph (Fig. 6), it can be observed that as CFV decreases, the predicted values (Eq. (e)) are not within the error bars of the observed values. Additionally, since Eq. (f) is for turbulent flow, using this equation in laminar and transitional flow regions resulted in significant errors in the predicted values.

Fig. 6 and Table 3 demonstrate the limitations of directly applying previously reported empirical Nusselt number equations for flux prediction in different systems. This is because previously reported empirical equations have difficulty incorporating the effects of geometric factors, such as variations in pipe size at the module inlet and fluid flow characteristics (horizontal or vertical inflow), which differ across systems (Ansari *et al*. 2021, Dudchenko *et al*. 2020, Hitsov *et al*. 2015). For this reason, modeling is performed using computational fluid dynamics (CFD). (Yazgan-Birgi *et al*. 2019). However, this approach is complex and consumes excessive time in modeling porous media, and a model that perfectly reflects heat transfer has not yet been established. (Ansari *et al*. 2021). Therefore, this study aims to present a useful method in the following section for enhancing the accuracy of flux predictions by empirically deriving Nusselt equation suitable for each system, considering the effects of fluid flow by distinguishing between laminar and transitional flow regions.

4.3 Empirical Determination of the Nusselt Number

Distillation experiments were conducted under various temperature and cross flow rate conditions to derive the Nusselt equation. The graph in Fig. 7 represents the heat transfer coefficient at various flow rates for each temperature condition.

The heat transfer coefficient varies depending on the system, so the constants a, b, and c in Eq. (10) need to be empirically determined (Kim *et al*. 2018). The relationship between heat transfer and CFV is provied below.

$$\mathrm{h} = \mathrm{A} \times CFV^{B} \tag{27}$$

As mentioned earlier, as the CFV increases, the thermal boundary layer becomes thinner, resulting in enhanced heat transfer efficiency (Hitsov *et al*. 2015, Yazgan-Birgi *et al*. 2019). Therefore, according to Eq. (27), h is proportional to CFV^{B}. The following equation can be expressed as follows by combining this functional relationship with Eqs. (10)-(15), (Kim *et al*. 2018).

$$\begin{aligned}\mathrm{Nu} = \frac{hd_h}{k} = \frac{A \times CFV^{B} d_h}{k} = aRe^{b}Pr^{c} \\ = a\left(\frac{CFV \times d_h\rho}{\mu}\right)^{b}\left(\frac{C_p\mu}{k}\right)^{c}\end{aligned} \tag{28}$$

First, when the heat transfer coefficient for CFV is fitted separately under laminar and transitional flow conditions at various temperature conditions, a linear relationship is observed, as shown in Fig. 7, with an R^2 value exceeding 0.9. Therefore, this study assumes a linear relationship between CFV and the heat transfer coefficient. According to the experimental results, it can be determined that B = b = 1 and c = 0.33 (Khayet *et al*. 2011). Therefore, 'a' can be calculated by using the following equation.

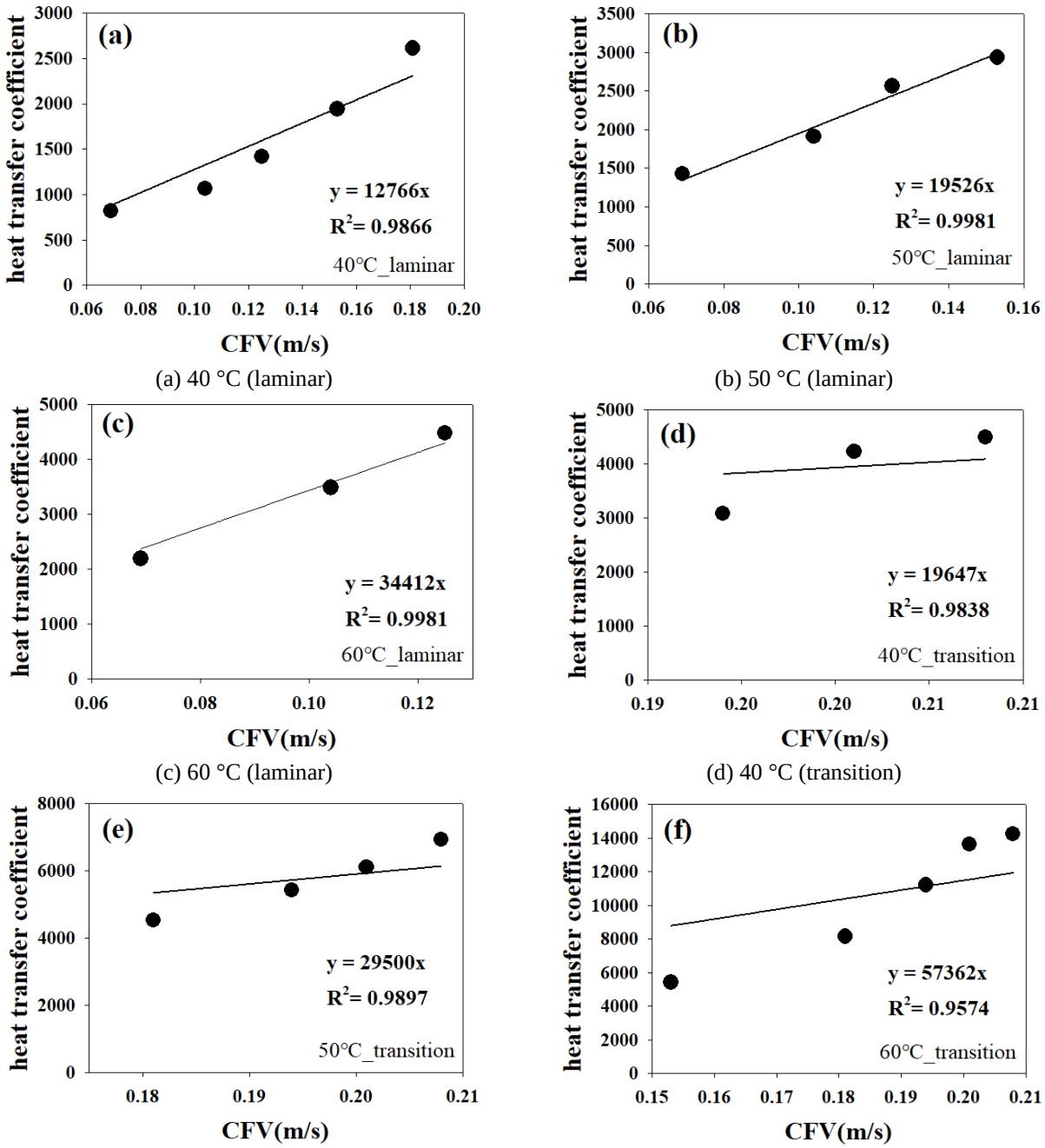

(a) 40 °C (laminar) (b) 50 °C (laminar)

(c) 60 °C (laminar) (d) 40 °C (transition)

(e) 50 °C (transition) (f) 60 °C (transition)

Fig. 7 Heat transfer coefficient (W/m^2·K) plotted as a function of CFV for feed temperatures of 40°C, 50°C, and 60°C using experimental data that distinguished between laminar and transition regions

$$a = A\, k^{-0.67} {d_h}^{0} \rho^{-1} \mu^{0.67} C_p^{-0.33} \quad (29)$$

The thermal conductivity (k) of water at temperatures of 20, 40, 50, and 60 °C is 0.596, 0.628, 0.640, and 0.651 W/m·K, respectively (Haynes 2016, Speight 2005). The hydraulic diameter (d_h) can be calculated by using Eq. (15), which is d_h= 0.007059 m. C_p represents the specific heat coefficient, and its values at 20, 40, 50, and 60 °C are 4184.4, 4179.6, 4181.5, and 4185.1 J/kg·K, respectively (Ļengel and Ghajar 2011, Incropera *et al*. 1996). ρ represents density, and μ stands for viscosity.

'A' was derived as 12,766, 19,526 and 34,412 as a result of regression of heat transfer coefficient at 40, 50, and 60 ℃ in the laminar layer, which are shown in Fig. 7(a)-(c). As reported in the previous literature, the heat transfer coefficient increased as the temperature increased (Termpiyakul *et al*. 2005). The regression equations fitted for the heat transfer coefficient concerning CFV showed R^2 values of 0.9866, 0.9981, and 0.9981 at temperatures of 40, 50, and 60 °C, respectively. The equation $y = 0.0023e^{0.0496T}$ was derived when fitting 'A' again as a function of temperature (K), which is shown in Fig. 8(a). 'a' for each temperature was

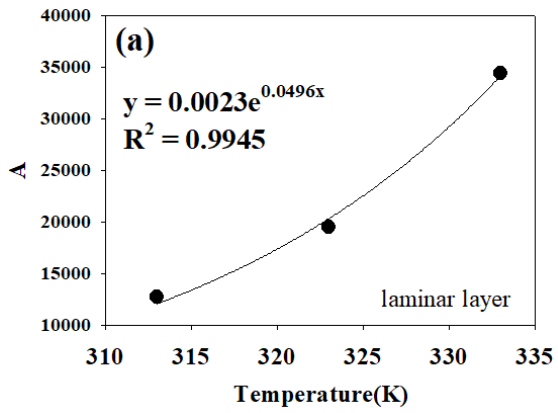

(a) The constant 'a' in the laminar layer

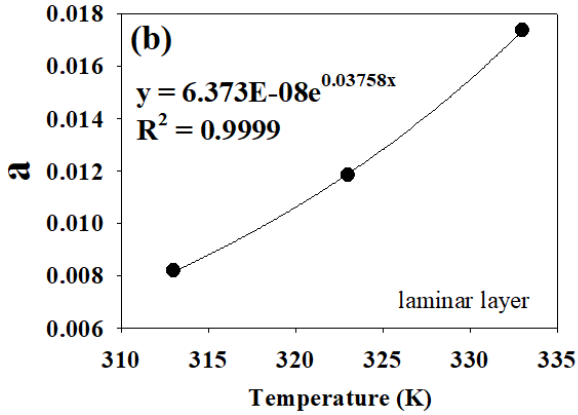

(b) The constant 'A' in the laminar layer

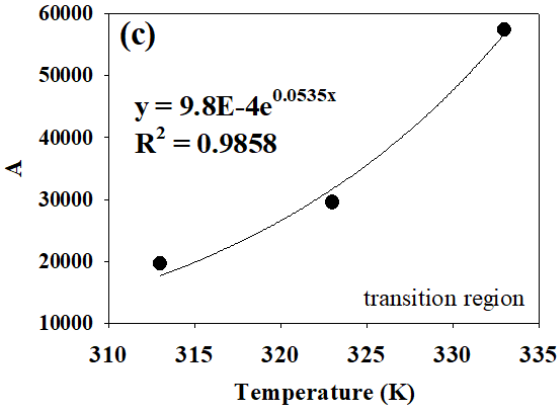

(c) The constant 'a' in the transition region

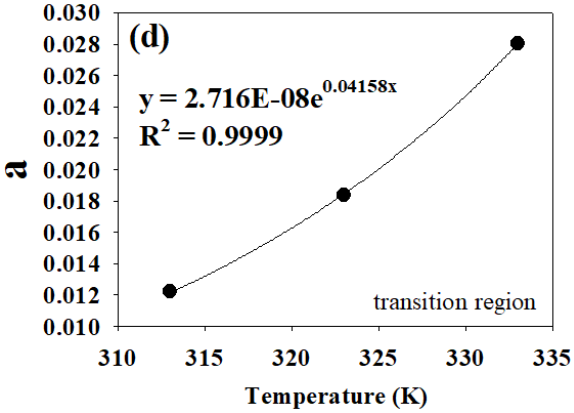

(d) The constant 'A' in the transition region

Fig. 8 The coefficients 'a' and 'A' were plotted as a function of temperature

computed by using Eq. (29). The graph of 'a' fitted against temperature is shown in Fig. 8(b). The function of $y = 6.373E-08e^{0.03758T}$ was derived (R^2=0.999). The Nusselt equation for the laminar layer, which was derived using the values of 'a,' 'b,' and 'c,' is provided below.

$$\text{Nu} = 6.373E-08e^{0.03758T}\ \text{Re}\ Pr^{0.33} \quad (30)$$

(laminar layer)

The results of the experiments conducted at three different temperatures in the transition region were fitted, and they resulted in values of 'A' as 19,647, 29,500, and 57,362, respectively which are displayed in Fig. 7(d)-(f). The regression equations fitted for the heat transfer coefficient concerning CFV showed R^2 values of 0.9838, 0.9879, and 0.9574 at temperatures of 40, 50, and 60 °C, respectively. The equation $y = 9.8E-4\ e^{0.0525T}$ was derived when fitting 'A' again as a function of temperature, which is shown in Fig. 8(c). The graph of 'a' fitted against temperature is shown in Fig. 8(d) (R^2 =0.999). The function of $y = 2.716E-08e^{0.04158T}$ was derived. The Nusselt equation for the transition region, which was derived using the values of 'a,' 'b,' and 'c,' is as follows:

$$\text{Nu} = 2.716E-08e^{0.04158T}\ \text{Re}\ Pr^{0.33} \quad (31)$$

(transition region)

Fig. 9 compares the observed flux with the predicted flux, calculated using empirical equations corresponding to the fluid regions that vary with each operating condition (CFV, temperature). The results showed that the predicted fluxes closely matched the observed values. Furthermore, the t-test analysis in Table 4 further validated that the developed model provided highly accurate flux estimates within a 5% significance level. Additionally, the MAPE of the observed values from the experiments conducted at 60 °C and the predicted values obtained using the developed Nusselt equation was 3%, which was higher than that of predictions made using existing Nusselt equations. As a result, by distinguishing between laminar and transitional flow regions using the method proposed in this study, it is possible to derive Nusselt empirical equations that are adapted to the specific conditions of the system and module, leading to more accurate flux predictions.

4.4 Evaluation of the predictability of flux

Additional experiments were conducted under different operating conditions to evaluate the predictability of the empirical Nu equation. The temperature condition on the feed side was 55 °C, and it was 20 °C on the permeate side. The fluxes were 12.01, 12.32, 13.39, 14.05, 15.44, 15.87, 16.01, and 16.63 L/m^{2}h at CFV of 0.069, 0.104, 0.125, 0.153, 0.181, 0.194, 0.201, and 0.208 m/s, respectively. The

Table 4 Statistical analysis (t-test) between the predicted and observed value at 40, 50, 60 ℃ (5% significance level, two-tail test)

	40 ℃		50		60 ℃	
	Predicted	Observed	Predicted	Observed	Predicted	Observed
Average	6.15	5.86	11.16	11.28	18.34	18.92
Variance	1.19	1.09	2.99	1.80	2.81	4.20
No. observations	8	8	8	8	8	8
Degree of freedom	7		7		7	
Null hypothesis, H_0	0		0		0	
t-value	5.72		-0.82		-3.30	
p-value	0.0007		0.436		0.013	

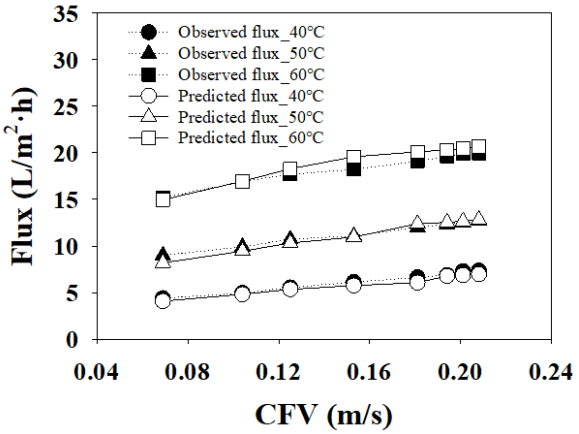

Fig. 9 Comparison between the observed flux and the predicted flux using the empirical Nusselt number that was derived from this study

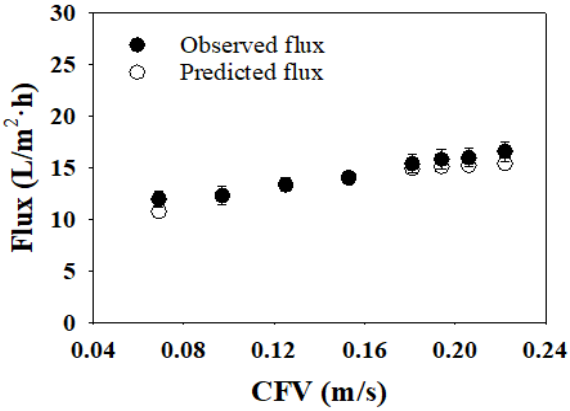

Fig. 10 Comparison between the observed values and the predicted values for a feed temperature of 55°C

predicted fluxes using the Nu empirical equation derived in this study are 10.82, 12.36, 13.40, 14.15, 15.44, 15.87, 16.01, and 16.63 L/m^2·h. Fig. 10 is a comparison of the predicted flux and the observed flux. The mean squared error (MSE) and the mean absolute percentage error (MAPE) were computed to assess the accuracy between the observed and predicted fluxes. MSE was 0.518, and MAPE was 3.79 %. It was confirmed that the predicted values closely match the observed values when using the newly derived Nusselt

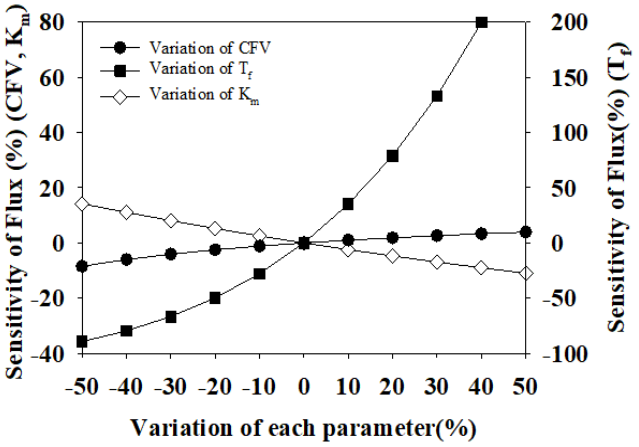

Fig. 11 Sensitivity of parameters on the predicted flux

equation for predicting flux. Moreover, the t-test analysis in Table 5 confirmed that the developed model produced highly accurate flux predictions, with a significance level of 5%.

A sensitivity analysis of flux was conducted by simulating the developed model with various parameter (CFV, the temperature of the feed, thermal conductivity of the membrane, Km) changes. The results are shown in Fig. 11. To verify that the sensitivity tests were conducted effectively, a sensitivity analysis was performed on the membrane characteristic parameter, specifically the thermal conductivity of the membraneAs the thermal conductivity of the membrane (K_m) varied from -50% to +50% of the initial value, the predicted change in flux ranged from 14% to -11%. As mentioned in the introduction, an increase in K_m leads to a reduction in flux due to heat loss (Q_c) caused by thermal conduction (Al-Obaidani *et al.* 2008). As the temperature of the feed varies from -50% to +50% of the initial value (60 °C), the flux is predicted to change between -89% and 280%. This result is expected, as an increase in feed temperature raises the vapor pressure, thereby enhancing the temperature gradient across the membrane that drives flux generation (Alkhudhiri *et al.* 2012, Phattaranawik *et al.* 2003b). As the CFV varies from -50% to +50% of the initial value (0.125 m/s), the flux is predicted to change between -8% and 4%. The results showed that a high CFV near the membrane surface disrupts the formation of temperature polarization within

Table 5 Statistical analysis (t-test) between the predicted and observed value at 55 ℃ (5% significance level, two-tail test)

	Predicted	Observed
Average	13.94	14.46
Variance	2.73	3.13
No. observations	8	8
Degree of freedom	7	
Null hypothesis, H_0	0	
t-value	-2.8	
p-value	0.026	

the boundary layer between the bulk solution and the membrane surface, leading to an increase in flux (Martínez-Díez and Vazquez-Gonzalez, 1999, Zhang *et al*. 2010). Additionally, within the vapor pressure range that can occur at the bulk temperature, a faster CFV leads to more efficient heat transfer, resulting in an increase in flux. In other words, an increase in CFV enhances the vapor pressure gradient across the membrane, but the absolute magnitude of heat transfer is determined by the bulk temperature (Dudchenko *et al*. 2020). For this reason, the feed solution temperature was found to be the most sensitive to the predicted flux compared to other parameters.

5. Conclusions

Heat transfer via each boundary layer acts as a limiting factor for the efficiency of DCMD. It is not possible to directly measure the temperature at the membrane's surface in DCMD process, so deriving the membrane surface temperature via heat transfer coefficients allows for the prediction of flux based on operating conditions. The heat transfer coefficient can be calculated via the Nusselt number. Membrane distillation experiments were conducted under various cross flow velocity and temperature conditions to derive an empirical Nusselt equation that is suitable for MD systems in this study. According to the experimental results, the Reynolds number increased as the CFV increased at the same temperature, which lead to an increase in the heat transfer coefficient. The observed heat transfer coefficient exhibited different trends in the laminar layer and the transition region based on the Reynolds number. Empirical Nusselt equations were consequently derived by distinguishing between these two regions, which are provided below.

$$\mathrm{Nu} = 6.373\mathrm{E}-08e^{0.03758T}\ \mathrm{Re}\ Pr^{0.33}$$

(laminar layer)

$$\mathrm{Nu} = 2.716\mathrm{E}-08e^{0.04158T}\ \mathrm{Re}\ Pr^{0.33}$$

(transition region)

The empirical Nusselt equation that was derived in this study can be employed to predict the flux in the direct contact membrane distillation process. In this study, Nusselt empirical equations were derived more easily by distinguishing between laminar and transitional flow regions, allowing for simpler and more accurate flux predictions adapted to the specific conditions of the system and module.This modeling approach can offer greater insights into the relationship between flux, cross flow velocity, temperature, and heat transfer.

Through experiments conducted under a wider range of temperature conditions beyond the tested range of this study (40 - 60 ℃) and at CFV values exceeding 0.208 m/s, empirical equations can be derived, enabling the development of a model that is applicable under broader operational conditions. Further experimental investigations should be conducted to derive a comprehensive model. The effects of geometric factors, such as changes in the size of the inlet pipe within the system, the fluid flow pattern (horizontal or vertical inflow) due to the module's internal structure, as well as the length and size of the module, have been indirectly reflected in the constants a, b, and c. However, by introducing each parameter into the empirical equation in the future, a more accurate understanding of the heat transfer relationship can be achieved.

Acknowledgments

This work was supported by the National Research Foundation of Korea (NRF) grant funded by the Korea government (MSIT) (RS-2023-00272506).

References

Abid, M.B., Wahab, R.A., Abdelsalam, M., Gzara, L. and Moujdin, I.A. (2023), "Desalination technologies, membrane distillation, and electrospinning, an overview", *Heliyon*, e12810. https://doi.org/10.1016/j.heliyon.2023.e12810

Al-Obaidani, S., Curcio, E., Macedonio, F., Di Profio, G., Al-Hinai, H. and Drioli, E. (2008), "Potential of membrane distillation in seawater desalination: Thermal efficiency, sensitivity study and cost estimation", *J. Membr. Sci*., **323**(1), 85-98. https://doi.org/10.1016/j.memsci.2008.06.006.

Alkhudhiri, A., Darwish, N. and Hilal, N. (2012), "Membrane distillation: A comprehensive review", *Desalination*, **287**, 2-18. https://doi.org/10.1016/j.desal.2011.08.027.

Andrjesdóttir, Ó., Ong, C.L., Nabavi, M., Paredes, S., Khalil, A., Michel, B. and Poulikakos, D. (2013), "An experimentally optimized model for heat and mass transfer in direct contact membrane distillation", *Int. J. Heat Mass Transf.*, **66**, 855-867. https://doi.org/10.1016/j.ijheatmasstransfer.2013.07.051.

Ansari, A., Kavousi, S., Helfer, F., Millar, G. and Thiel, D.V. (2021), "An improved modelling approach for the comprehensive study of direct contact membrane distillation", *Membranes*, **11**(5), 308. https://doi.org/10.3390/membranes11050308

Bergman, T.L., Bergman, T.L., Incropera, F.P., Dewitt, D.P. and Lavine, A.S. (2011), *Fundamentals of Heat and Mass Transfer*, John Wiley & Sons.

Chauhan, K.S. and Tyagi, H. (2023), "Thermal modeling of fluid flow and heat transfer in direct contact membrane distillation", *Energy Convers. Manage*., **291**, 117249. https://doi.org/10.1016/j.enconman.2023.117249.

Choi, J., Cho, J., Shin, J., Cha, H., Jung, J. and Song, K.G. (2022), "Performance and economic analysis of a solar membrane distillation pilot plant under various operating conditions", *Energy Convers. Manage*., **268**, 115991. https://doi.org/10.1016/j.enconman.2022.115991.

Curcio, E. and Drioli, E. (2005), "Membrane distillation and related operations—a review", *Sep. Purif. Rev.*, **34**(1), 35-86. https://doi.org/10.1081/SPM-200054951.

Drioli, E., Ali, A. and Macedonio, F. (2015), "Membrane distillation: Recent developments and perspectives", *Desalination*, **356**, 56-84. https://doi.org/10.1016/j.desal.2014.10.028.

Dudchenko, A.V., Hardikar, M., Xin, R., Joshi, S., Wang, R., Sharma, N. and Mauter, M.S. (2020), "Impact of module design on heat transfer in membrane distillation", *J. Membr. Sci.*, **601**, 117898. https://doi.org/10.1016/j.memsci.2020.117898

González, D., Amigo, J. and Suárez, F. (2017), "Membrane distillation: Perspectives for sustainable and improved desalination", *Renew. Sust. Energy Rev.*, **80**, 238-259. https://doi.org/10.1016/j.rser.2017.05.078.

Gryta, M. and Tomaszewska, M. (1998), "Heat transport in the membrane distillation process", *J. Membr. Sci.*, **144**(1-2), 211-222. https://doi.org/10.1016/S0376-7388(98)00050-7.

Gryta, M., Tomaszewska, M. and Morawski, A. (1997), "Membrane distillation with laminar flow", *Sep. Purif. Technol.*, **11**(2), 93-101. https://doi.org/10.1016/S1383-5866(97)00002-6.

Haynes, W.M. (2016), *CRC Handbook of Chemistry and Physics*, CRC press, Boca Raton, Florida, USA, Boca Raton, Florida, U.S.A.

Hitsov, I., Maere, T., De Sitter, K., Dotremont, C. and Nopens, I. (2015), "Modelling approaches in membrane distillation: A critical review", *Sep. Purif. Technol.*, **142**, 48-64. https://doi.org/10.1016/j.seppur.2014.12.026

Įengel, Y. and Ghajar, A.J. (2011), "Heat and Mass Transfer: Fundamentals & Applications", McGraw-Hill, New York, U.S.A.

Incropera, F.P., DeWitt, D.P., Bergman, T.L. and Lavine, A.S. (1996), *Fundamentals of Heat and Mass Transfer*, Wiley New York, New York, N.Y., U.S.A.

Izquierdo-Gil, M.A., Fernández-Pineda, C. and Lorenz, M. (2008), "Flow rate influence on direct contact membrane distillation experiments: Different empirical correlations for Nusselt number", *J. Membr. Sci.*, **321**(2), 356-363. https://doi.org/10.1016/j.memsci.2008.05.018.

Khayet, M. and Matsuura, T. (2011), *Membrane Distillation*, Elsevier.

Khayet, M., Souhaimi, M.K. and Matsuura, T. (2011), *Membrane Distillation: Principles and Applications*, Elsevier.

Khayet, M., Velázquez, A. and Mengual, J.I. (2004), "Modelling mass transport through a porous partition: effect of pore size distribution", *J. Non Equil. Thermodyn.*, **29**(3), 279-299. https://doi.org/10.1515/JNETDY.2004.055.

Kim, S., Kim, S., Ahmed, Z., Cha, D.K. and Cho, J. (2018), "Flux model for the membrane distillation process to treat wastewater: Effect of solids concentration", *J. Membr. Sci.*, **566**, 396-405. https://doi.org/10.1016/j.memsci.2018.09.018.

Kim, S., Park, K.Y. and Cho, J. (2017), "Evaluation of the efficiency of cleaning method in direct contact membrane distillation of digested livestock wastewater", *Membr. Water Treat.*, **8**(2), 113-123. https://doi.org/10.12989/mwt.2017.8.2.113.

Lawal, D.U. and Khalifa, A.E. (2014), "Flux prediction in direct contact membrane distillation", *Int. J. Mater. Mech. Manuf.*, **2**(4), 302-308. https://doi.org/10.7763/IJMMM.2014.V2.147.

Lawson, K.W. and Lloyd, D.R. (1997), "Membrane distillation", *J. Membr. Sci.*, **124**(1), 1-25. https://doi.org/10.1016/S0376-7388(96)00236-0.

Leitch, M.E., Lowry, G.V. and Mauter, M.S. (2017), "Characterizing convective heat transfer coefficients in membrane distillation cassettes", *J. Membr. Sci.*, **538**, 108-121. https://doi.org/10.1016/j.memsci.2017.05.028

Loussif, N. and Orfi, J. (2016), "Comparative study of air gap, direct contact and sweeping gas membrane distillation configurations", *Membr. Water Treat.*, **7**(1), 71-86. https://doi.org/10.12989/mwt.2016.7.1.071.

Martínez-Díez, L. and Vazquez-Gonzalez, M.I. (1999), "Temperature and concentration polarization in membrane distillation of aqueous salt solutions", *J. Membr. Sci.*, **156**(2), 265-273. https://doi.org/10.1016/S0376-7388(98)00349-4.

Moreira, V.R., Lebron, Y.A.R. and Amaral, M.C.S. (2022), "Enhancing industries exploitation: Integrated and hybrid membrane separation processes applied to industrial effluents beyond the treatment for disposal", *Chem. Eng. J.*, **430**, 133006. https://doi.org/10.1016/j.cej.2021.133006.

Moreira, V.R., Raad, J.V., Lazarini, J.X., Santos, L.V. and Amaral, M.C. (2023), "Recent progress in membrane distillation configurations powered by renewable energy sources and waste heat", *J. Water Proc. Eng.*, **53**, 103816. https://doi.org/10.1016/j.jwpe.2023.103816.

Phattaranawik, J., Jiraratananon, R. and Fane, A. (2003a), "Effect of pore size distribution and air flux on mass transport in direct contact membrane distillation", *J. Membr. Sci.*, **215**(1-2), 75-85. https://doi.org/10.1016/S0376-7388(02)00603-8.

Phattaranawik, J., Jiraratananon, R. and Fane, A.G. (2003b), "Heat transport and membrane distillation coefficients in direct contact membrane distillation", *J. Membr. Sci.*, **212**(1-2), 177-193. https://doi.org/10.1016/S0376-7388(02)00498-2.

Schofield, R., Fane, A. and Fell, C. (1987), "Heat and mass transfer in membrane distillation", *J. Membr. Sci.*, **33**(3), 299-313. https://doi.org/10.1016/S0376-7388(00)80287-2.

Shin, B., Shin, J., Wirasembada, Y.C., So, H. and Cho, J. (2024), "Predicting the flux of various volatile fatty acids mixtures in a membrane distillation", *Desalination* **583**, 117664. https://doi.org/10.1016/j.desal.2024.117664

Sieder, E.N. and Tate, G.E. (1936), "Heat transfer and pressure drop of liquids in tubes", *Ind. Eng. Chem.*, **28**(12), 1429-1435. https://doi.org/10.1021/ie50324a027.

Speight, J. (2005), *Lange's Handbook of Chemistry*, McGraw-Hill Education.

Srisurichan, S., Jiraratananon, R. and Fane, A. (2006), "Mass transfer mechanisms and transport resistances in direct contact membrane distillation process", *J. Membr. Sci.*, **277**(1-2), 186-194. https://doi.org/10.1016/j.memsci.2005.10.028.

Tai, Z.S., Othman, M.H.D., Koo, K.N. and Jaafar, J. (2023), "Critical review on membrane designs for enhanced flux performance in membrane distillation", *Desalination*, **553**, 116484. https://doi.org/10.1016/j.desal.2023.116484.

Termpiyakul, P., Jiraratananon, R. and Srisurichan, S. (2005), "Heat and mass transfer characteristics of a direct contact membrane distillation process for desalination", *Desalination*, **177**(1-3), 133-141. https://doi.org/10.1016/j.desal.2004.11.019.

Thomas, L. (1992), *Heat Transfer. Ed*, Prentice-Hall, Englewood Cliffs, New Jersey, U.S.A.

Tibi, F., Charfi, A., Cho, J. and Kim, J. (2020), "Fabrication of polymeric membranes for membrane distillation process and application for wastewater treatment: Critical review", *Proc. Safe. Environ. Protect.*, **141**, 190-201. https://doi.org/10.1016/j.psep.2020.05.026.

Wang, Y., Liu, X., Ge, J., Li, J. and Jin, Y. (2023), "Distillation performance in a novel minichannel membrane distillation device", *Chem. Eng. J.*, **462**, 142335. https://doi.org/10.1016/j.cej.2023.142335.

Yazgan-Birgi, P., Ali, M.I.H. and Arafat, H.A. (2019), "Comparative performance assessment of flat sheet and hollow fiber DCMD processes using CFD modeling", *Sep. Purif. Technol.*, **212**, 709-722. https://doi.org/10.1016/j.seppur.2018.11.085

Yunus, A.Ç. (2019), *Heat and Mass Transfer: Fundamentals and Applications*, McGraw-Hill Education.

Zhang, J., Dow, N., Duke, M., Ostarcevic, E. and Gray, S. (2010), "Identification of material and physical features of membrane distillation membranes for high performance desalination", *J. Membr. Sci*., **349**(1-2), 295-303. https://doi.org/10.1016/j.memsci.2009.11.056

KC